MAEV
*M*artian *A*irborne *E*xploration *V*ehicle

Wichita State University
Department of Aerospace Engineering

HEDS-UP Forum
May 2000

Manager:
Ravi Malla

MAEV Team Members:
Soo Han Loo
Loy Yik Liew
Ng Seet Wai
Dean Edmonston
Truong Dinh
Nishanka Mahathalagalage

Martian Exploration Parachute
Chuong Dinh
Roberto Medina-Fernandez
Jaime Gavino-Nadal

Faculty Advisor:
Dr. M. Gawad Nagati

Abstract:

A conceptual approach was taken to design an airborne exploration vehicle capable of operating in the Martian atmosphere. To complete the design, a modular Carriage and Track system capable of deploying and retrieving the aircraft was also developed. Known as the Martian Airborne Exploration Vehicle, it is a solar powered wing body design with a span of 30.5 meters and a chord of 1.2 meters. With a full payload of 30 N, it weighs 300 N on Mars and has 4 propellers, which are capable of generating enough thrust to reach a maximum velocity of 67 m/s at a maximum altitude of 500 meters. The maximum radius of operation at the equator is 1000 kilometers. A 60-meter long Carriage and Track system fastened to the ground will be able to deploy the MAEV using a rocket assisted takeoff process, and then retrieve it using a resistance pulley mechanism.

TABLE OF CONTENTS

LIST OF TABLES

LIST OF FIGURES

1. Introduction

The success of human presence on Mars will critically rely on several factors. Among the most important ones is the ability for humans to have exploration capability on the planet. The prospect of successful missions to Mars has raised more questions than answers, in relation to what we need to know about our neighboring planet. With this in mind, a concept of an up-close, yet long range, exploration vehicle was conceived.

Due to the adverse geological construction of the planet, the range of surveillance should not be limited by the unpredictability of the terrain. An airborne craft will be suitable in meeting the demands of such missions. With a plan for the future, several considerations were taken into account, and after making logical assumptions, a conceptual aircraft was designed. Also, due to the unavailability and the difficulty in construction of a landing strip, a concept of a landing and takeoff track system was developed.

2. Initial Assumptions

The following assumptions made were critical in conceiving the MAEV design.

- Forecasting successful space travel in the next 20-30 years
- Capability of mass transportation of parts and components
- Long term human habitation
- Light scale manufacturing capability on Mars
- Availability of engineers to assemble and maintain the aircraft system
- Reliability of current planetary data and their accuracy
- Ability of forecasting of Martian weather
- Availability of lightweight avionics and laser precise telemetry equipment
- Dependability of stability augmentation and guidance system for aircraft

3. Approach

To create such an exploration aircraft system, several factors involving atmospheric differences between Earth and Mars were taken into consideration. The lesser gravity and considerably lower atmospheric density on Mars were the key components. To produce a feasible design, fundamental aspects of aircraft theory were assessed. These key categories include:

Aerodynamics:	Finding an aerodynamically capable and suitable airfoil configuration for the aircraft wing.
Power (Source/Supply):	Utilizing solar or forms of reusable power sources.
Propulsion:	Designing highly efficient propellers to provide thrust and solid rockets for assisted take-off.
Structures:	Using ultra light, yet strong materials to construct the aircraft.
Control & Avionics:	Application of highly accurate control and telemetry systems for maneuvering, landing and take off.

Focusing on each category, the fundamentals were addressed, and concepts meeting the criteria were developed. Analyses of individual components were completed to evaluate the feasibility of the final design.

4. Description

The current stage of the MAEV design consists of two major components: the aircraft itself, and the takeoff & landing track system. The aircraft has a wing body configuration with a span of 30.5 meters and a chord of 1.2 meters. The resulting aspect ratio is 25.42 with a wing area of 36.59 square meters. The aircraft itself consists of a solar array, 4 double blade propellers, lightweight electric engines (off-the-shelf motors), a rechargeable battery pack, avionics, control systems and predetermined weight room for payload. A detailed list of these components including the aerodynamic specifications, weight and dimensions of the aircraft are shown in Table 1.

Table 1. Component details of the MAEV

Components	Sub-components	Mars		Dimensions (m)
		Newtons	Kilograms	
Wing (structure)	Wing Skin			2.3×10^{-5} thick
	Circular Spar			0.1 dia., 30.5m length
	Airfoil Rib			
	Truss Member Rib			
	Prop Engine Supports			
	sub-total	104.4	28.0	30.5m x 1.2m
Engines & Prop (4)		37.2	10.0	1.4 m dia. Prop
Solar Array		98.1	26.3	17.5 m^2
Battery Pack		22.4	6.0	Variable (small)
Payload		29.8	8.0	Variable
Avionics		7.5	2.0	Variable (small)
Total Weight		**300.0**	**80.5**	**36.6 m^2**

The overall weight of 300 N includes secondary parts such as wiring and fasteners, which are assumed to be insignificant compared to their primary components. An exterior view of the wing body is shown below in Figure 1.

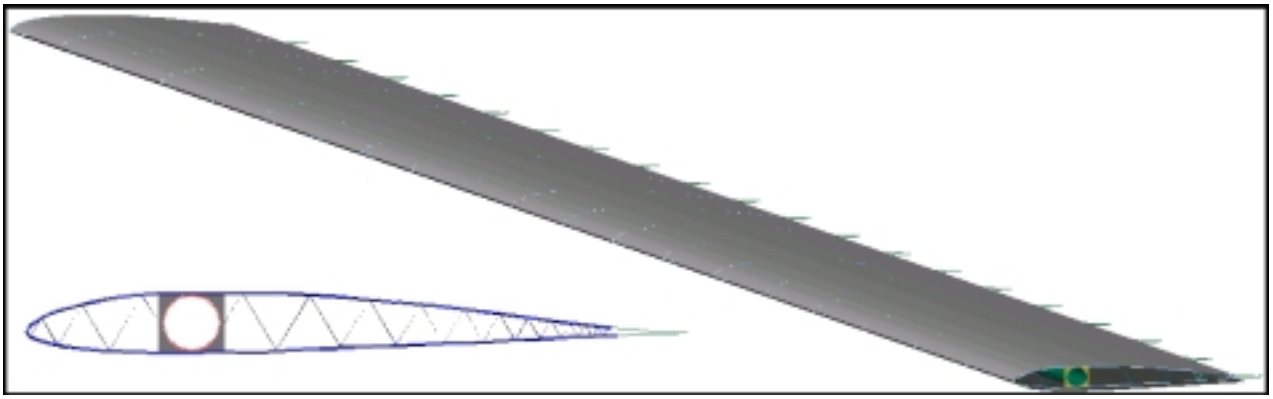

Figure 1. Exterior view of the wing body design

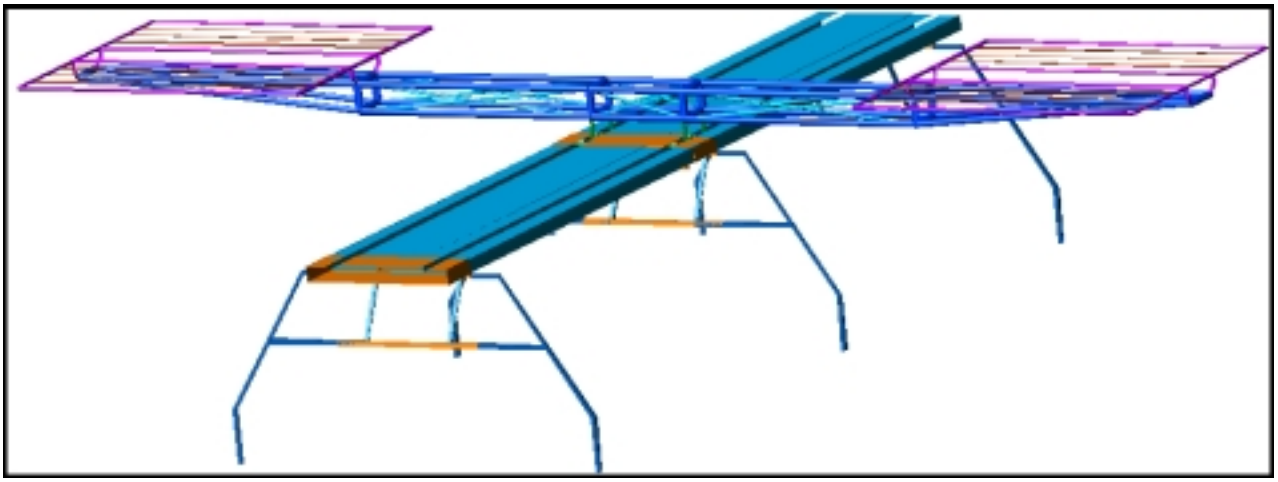

Figure 2. Carriage and Track system for aircraft landing and takeoff

For the takeoff and landing process, a track and carriage system as shown in Figure 2 was developed. Designed to be lightweight yet structurally stable, it is constructed mostly of Aluminum 6061 –T6. The specific dimensions and its details are shown below in Table 2.

Table 2. Component details of the Carriage and Track system

Components	Sub-components	Mars		Dimensions (m)
		Newtons	Kilograms	
Carriage	Carriage support	98.5	26.5	6 x 0.5 x 0.15
	wing supports			1.5 x 1.5 x 0.1
	wheel support			0.5 x 0.15
Track System	Main track module	58.0	15.6	0.75 x 0.1 x 3.0
	Main support			
	Outrigger support			
	Ground Support			
Total Weight		**156.5**	**42.0**	

4.1. AIRFOIL SELECTION

To obtain a suitable airfoil, the atmospheric data conditions of Mars were collected and analyzed. The key factors were the air density, the gravity and the air viscosity. Table 3 and 4 below lists these values.

The MH62 airfoil selected for the wing has a maximum lift coefficient, C_{Lmax} of 1.111 and parasite drag coefficient, C_{do} of 0.01332. It also has low moment coefficient, which is suitable for flying wing design. The trailing edge reflex of the airfoil tends to drive the pitching moment to be zero, allowing an aircraft configuration without a tail.

Table 3. Martian Atmospheric Data

Air density of Mars @ altitude 500 m	:	$\rho = 0.0144$ kg/m^3
Air density of Mars @ Sea Level	:	$\rho = 0.0150$ kg/m^3
Air viscosity of Mars	:	$\mu = 1.08 \times 10^{-5}$ N.s/m^2
Gravity of Mars	:	g = 3.7278 kg.m/s^2
Speed of Sound on Mars	:	a = 200 m/s

Table 4. Density Gradient Formula for Mars

For $h < 7000$

$T = -31 - 0.000998 * h$

$P = 0.699 * e^{-0.0009 * h}$

$R = p / (0.1921 * (T + 273.1))$

Where :

R = Density (kg/m^3)
P = Pressure (Pa)
T = Temperature (°C)

The MAEV is designed to have a maximum cruising velocity of 66m/s and a possible minimum velocity of 28 m/s. The operating Reynolds Number is around 100,000. The best lift to drag ratio cruising velocity for the current aircraft configuration is at 42 m/s. During takeoff conditions, with a full payload of 30N, the stall speed at sea level is 31.4 m/s and, during landing, the stall speed is 30 m/s, assuming that the payload has been jettisoned. The rate of climb of the MAEV at the maximum velocity of 67 m/s is 0.5 m/s and the best rate f climb of 2 m/s occurs at a velocity of 60 m/s. These values are, however, based on steady flight conditions.

4.2. PROPELLER DESIGN

To provide the thrust required for the MAEV, a highly efficient propeller is needed. The design chosen for this purpose, is a GM-15 airfoil, which has a low Reynolds number and high lift coefficient with moderately low drag coefficient. It has a maximum lift coefficient of 1.32 at an angle of attack of 16 degrees and a low Reynolds's number of 40000. The propeller is designed using detailed steps involving basic aerodynamic principles. Applying known values of the Martian atmosphere, a program was written.

Section	r, m	dr, m	Twist angle degree
1	0.03048	0.06096	89.989
2	0.09144	0.06096	79.241
3	0.1524	0.06096	68.116
4	0.21336	0.06096	59.064
5	0.27432	0.06096	51.903
6	0.33528	0.06096	46.232
7	0.39624	0.06096	41.763
8	0.4572	0.06096	38.154
9	0.51816	0.06096	35.175
10	0.542544	0.06096	34.144

Table 5. The r and β values for each segments

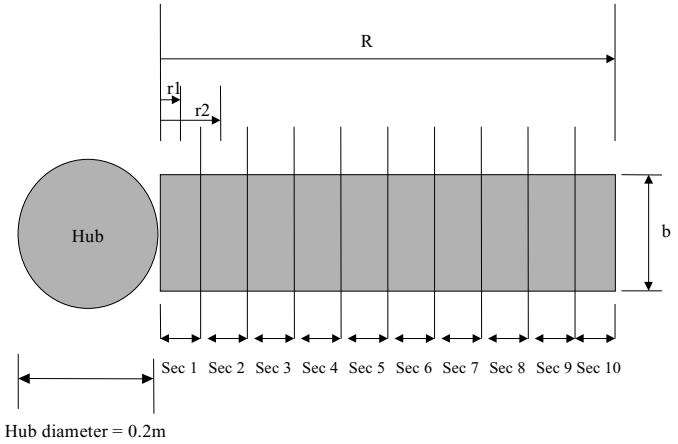

Figure 3. Configurations of a propeller blade

The radius of the propeller was divided into 10 equal length segments to find the best twist angle/geometric pitch angle from tip to root of the propeller. The gradient of the C_L versus α graph for GM 15 airfoil is $a_o = 0.1415$. The radius of the propeller is r = 0.6096m. The number of propeller blades is defined as B = 2. The chord length of the entire airfoil for the propeller is b = 0.1m with a hub radius of 0.1 m.

The thrust required for the aircraft was obtained. The angle of attack where the highest C_L/C_D value during cruise velocity was determined. The speed range of the MAEV was obtained and a speed was selected. A reasonable value for the revolution per seconds, n, was chosen. A trial and error method was conducted to estimate the twist angle, β, for all ten segments of the propeller blade based on the selected MAEV flying cruise speed. The effective pitch angle, ϕ, and the angle of attack, α, were calculated. The C_L and C_D values for lift and drag coefficients were taken from graphs for GM-15 airfoil. The values of the induced angle, θ, was determined and used to find ϕ_o. By limiting the tip speed of the propeller to 200 m/s, the relative velocity, V_R, was calculated. The thrust and torque was then determined. These steps were repeated for each of the ten segments. The r-values and the angle of twist values are shown in Table 5.

The next steps involved calculating the thrust and torque required at cruise speed. With the thrust found for one propeller, the total thrust produced by four propellers was determined. By applying a tip loss factor, 2% of the propeller length is deducted from the tip segment to calculate the actual thrust each propeller can produce. With the total thrust produced by 4 propellers (varying n to achieve the required thrust), the thrust produced can be matched to the thrust required. With this, the different velocity's power requirement to run the propellers was calculated. The propeller efficiency, P_{output}, P_{input}, and the efficiency, η, was then calculated. Additionally, the aspect ratio was calculated. The best performance of GM-15 airfoil is at the angle of attack of 9 degrees. The total thrust produce by 4 propellers at

different velocity was shown in Figure 4 and 5. Due to the need in changing the rps of the propeller to increase the free stream velocity, a gear mechanism for calculation purpose is required. The power required and the efficiencies to run 4 propellers at various velocities are shown in Figure 6 and 7.

The Aspect Ratio for the propeller is 12.2. The changes of thrust produced and required, power required and efficiency of the propeller can be seen in Figure 4, 5, 6 and 7, below. As shown in Figure 4, with a motor speed control system (for calculation purpose only), the propellers were only capable of cruising at the speed where the thrust required and thrust available intersect. The available cruising speed as shown in Figure 4 are 45m/s, 67m/s and 50 m/s. If avionics control systems are used to control the power input to the propellers, the cruising speed would be from 31m/s to 67m/s. The power required ranges from 502.866 W to 1366.4 W. This is mainly due to the capability of the control system in changing the revolution per second of the propellers. This can be seen in Figure 5. As a result, the propeller drawing with actual twist angle and its configuration is shown in Figure 8.

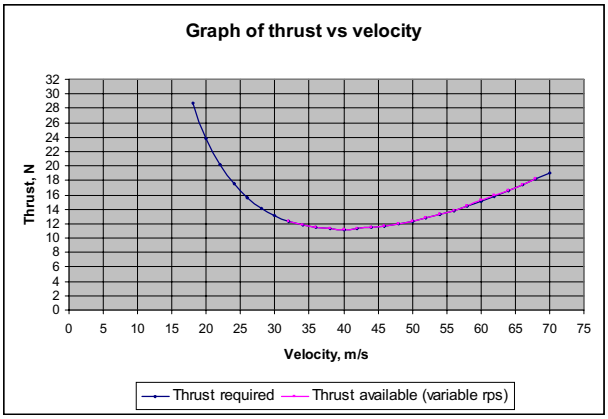

Figure 4. Graph of T_{ave} and T_{req} vs. V (MSC)

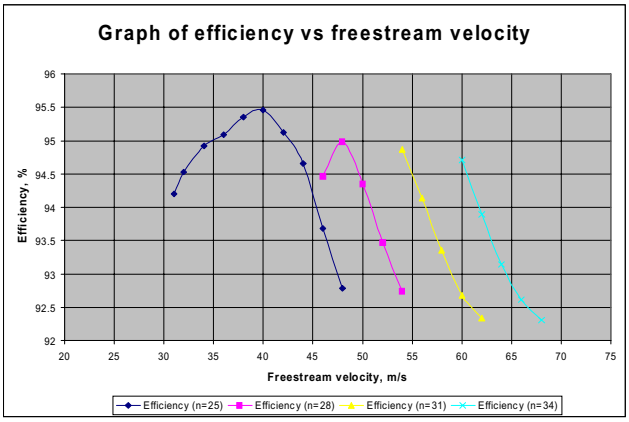

Figure 5. Graph of T_{ave} and T_{req} vs. V (a.c.s)

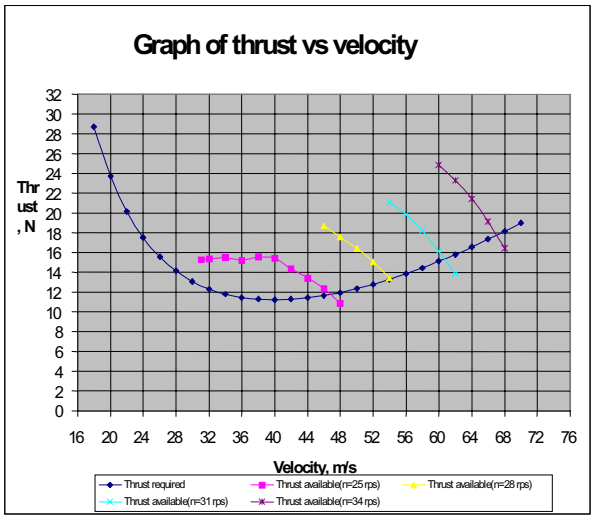

Figure 6. Graph of η_{prop} versus V

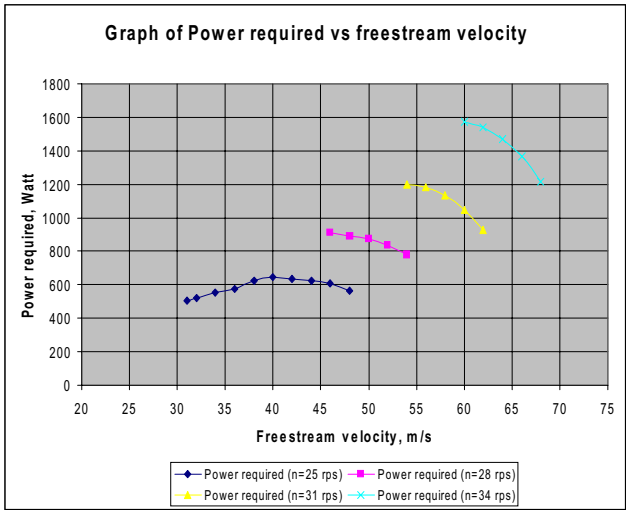

Figure 7. Graph of P_{req} vs V

The results show that the effective pitch angle is increasing from tip to root of the propeller. The n generated by this double blade propeller is reasonable as it provides an average of about 3500rpm rotation with the tip velocity (maximum tip speed = 130.245 m/s) not exceeding the speed of sound in Mars. Due to the low average operating Reynolds number of the propellers (Re # = 7611.278 to 12598.072), the GM-15 airfoil (Re # = 40,000) used for these calculations are not very accurate. The reason other airfoils were not chosen is because the GM-15 airfoil is the only low Reynolds number airfoil available with accurate data. Modifications on the airfoil, n, size, twist angle will help improve the efficiency of the propeller.

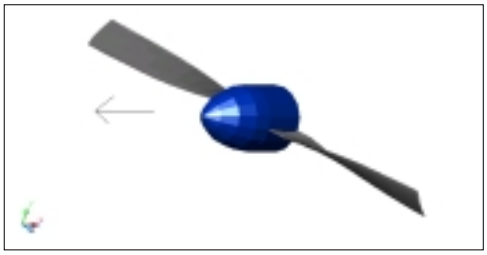

Figure 8.CAD Drawing of Designed Propeller

4.3. POWER

To meet the power requirement for the MAEV, two types of power sources were selected. One is a photovoltaic solar array, which utilizes solar energy in the form of photons converting light into electrical energy. The second power source is a rechargeable battery pack with a high energy density. These batteries can also be dedicated as backup power during solar array malfunctions. This precaution is taken due to the harshness of the Martian atmosphere.

4.3.1. Solar Array

Mars has lower light intensity of 0.4306 compared to 1.0 on Earth. The solar cells that are used on the MAEV are the dual-junction Gallium-indium-phosphorous/Gallium-Arsenide with Germanium substrate or $GaInP_2/GaAs/Ge$. The particular solar cell has an intensity (power per surface area) of $266W/m^2$ and mass per surface area of $1.51kg/m^2$ with efficiency currently stands at 21.5%. The solar array can survive 10-15 years of mission environment as claimed by Hughes Spectrolab.

The power requirement from the electric motor ranges from 560~1500 Watts depending on the speed and rpm of the propeller The maximum power output from the solar array is 2000W. This covers an area of $17.5m^2$ on top of the $36.6m^2$ wing area. The weight of the solar array is 26.3kg or 98.1N in Mars. (Note that the solar array area can be increased to generate more power, however, increasing the area in turn would pay a heavy weight penalty). The excess power from the solar array is directed to other electric components in the aircraft such as avionics and payload equipment (example, spectrometer, imaging instrument, communication devices, micro probes etc.).

4.3.2. Rechargeable Battery Pack

A rechargeable Silver-Zinc battery pack is the second types of power source selected for the MAEV. The aircraft is designed to carry 6 cells of this type, which weigh 1kg each, in parallel configuration instead of a series for a fail-safe reason. Silver-Zinc has a high power density and a discharge rate of 176W.hr/kg and 320A.hr respectively. It is a rugged, leak proof and spill proof design, which can operate in very cold temperatures ($+70^0$C to -21^0C) and can be packaged in the most severe requirements. The recharge time is 8 hours with and the life span is 200 charges.

The power generated by the solar array is heavily dependent on the angle of the sun with respect to the aircraft's upper surface and the latitude of operation. Table 6 shows the variance in performance with respect to the power produced at a given operation time frame. These values are based on a zero degree Martian latitude operation.

Table 6. Variable cruise velocity with respect to power generated by solar array

Flight time in hours	Power produced at particular time frame(Watts)	Minimum power required with respect to velocity(Watts)	Cruise velocity (m/s)	Distance traveled(km)
0800-0900	911	673	46	165.6
0900-1000	1332	1260	58	208.8
1000-1600	1831	1520	66	1,425.6
1600-1700	1177	931	52	187.2

(Note: This situation only refers for 0-degree latitude)

4.4. RANGE OF OPERATION

Relying on just the Solar Array, the MAEV has a flight distance of 2000 km and a flight time of 9 hours at 0-degree latitude. The maximum distance capable at a latitude range of 0 to 60 is shown in Table 7 below. It also shows the maximum flight time possible for each 10-degree increment. The maximum range of the aircraft is deduced from a best cruise velocity combination, which is dependent on the time of day. An example is shown in Table 6 above.

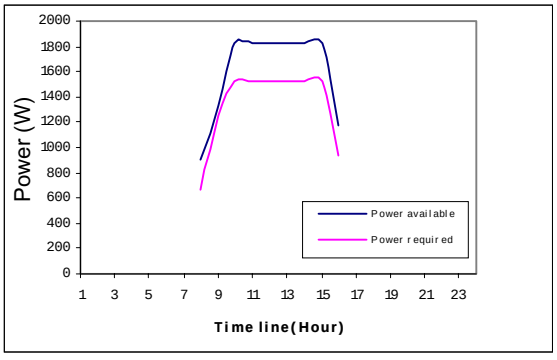

Figure 9. Power Available vs. Required

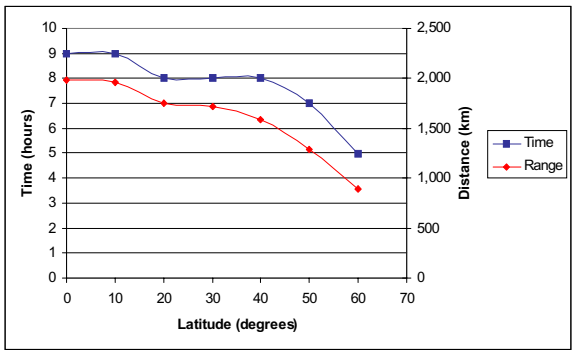

Figure 10. Operation hours & distance traveled

Increasing the cruise velocity will greatly improve the range, therefore, batteries can be used as a supplemental power source to maintain a cruise speed of 66m/s during the entire flight. Maintaining a cruise speed of 66m/s requires constant power of 1520W. Thus, the rechargeable Silver-Zinc batteries can compensate the deficiency in power at certain flight time frames. Table 7 summarizes the battery usage in attempting to maintain the 66m/s cruise speed.

Table 7. Batteries integration to maintain highest cruise velocity

Cruise velocity(m/s)	Power required w.r.t. velocity(W)	Power demand to maintain 66m/s (W)	Batteries required	Power supplied by batteries (W)
52 @ 0800	931	589	4	704
58 @ 0900	1260	260	2	352
66 @ 1000	1520	0	Not required	0

(Note: This situation only refers for 0-degree latitude)

By utilizing the battery pack in sequence with the solar array, an increase of 79-km flight distance can be achieved. Also, the MAEV will be able to operate anywhere within –60 to +60 degrees of latitude on the Martian atmosphere as long as the solar exposure is equal on both hemispheres.

4.5. Design of Carriage and Track System

A system for taking-off and landing the MAEV on the Martian surface is proposed here. Due to the harsh geological environment on the Martian surface, runways are unrealistic during early exploration. A take-off and landing apparatus has been proposed which can adapt to the terrain on which it is erected. The system consists of two main systems: a track and a carriage system. Each main system consists of several subsystems that are described below.

4.5.1. Carriage System

The carriage system is a detachable landing gear for use during departure and landing. The system has three subsystems, the wing supports, the carriage supports, and the wheel supports. The aircraft is designed to take-off and land in the same direction.

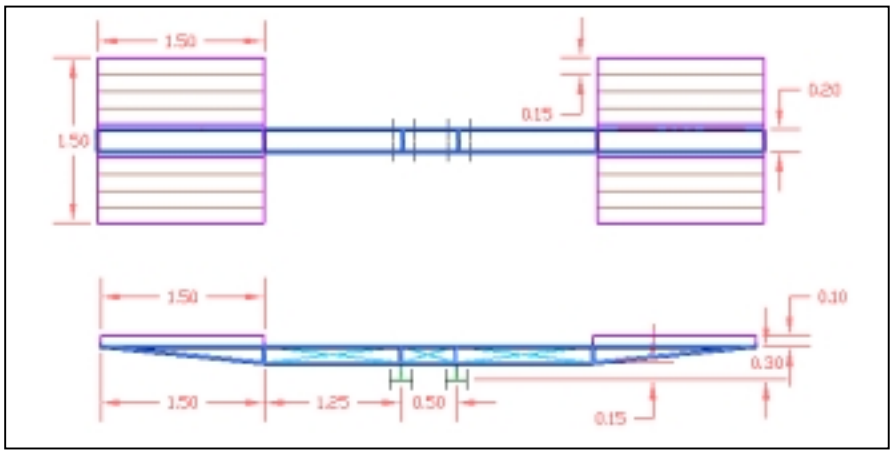

Figure 11 Drawing of Carriage System

4.5.2. Carriage Subsystems

Carriage Wheel System

The wheel system is designed to translate the carriage system to one direction. The wheel system is confined by the track and provides unidirectional travel during take-off and landing. A dual track monorail has been proposed for stability and resistance to bending loads.

Carriage Wing Support System

The wing support system is designed to restrain the aircraft during acceleration and deceleration associated with T-O and landing, respectively. To restrain the aircraft, the wing supports are fitted with end caps that are free to rotate 90° and lock into place. To secure the vehicle to the supports, magnets have been purposed. Magnetic force can be used to secure the aircraft during take-off until the vehicle has attained a velocity to induce lift. During landing, magnets can be used to secure and align the vehicle with the supports. Magnets will be carried on the wing support subsystem and metal strips placed on the exterior of the vehicle.

Carriage Support System

The carriage supports provide structural rigidity for the wing supports. The carriage support is a truss frame that resists bending loads due to the weight of the vehicle on the wing supports.

4.5.3. *Track System*

The track system is a portable, adjustable runway for the MAEV vehicle. The track system is designed to support the carriage system and the aircraft during take-off and landing. Additionally, the system must be easily transported, erected, and maintained on the Martian surface by a two person's crew. The track system consists of two subsystems, the main track, which houses the carriage wheel subsystem and the track support system.

The length of the overall track will need to be 50+ meters long. To provide this length, the track is designed to be modular, connecting several tracks together for the required length. Special consideration was also given to non-structural problems including ease of transport and set-up, ground restraints, module interfacing, and dust contamination control. The maximum overall dimensions of the system are 1.6-m high, 1.95-m wide and 3.0-m long. The maximum dimensions are for fully extended supports.

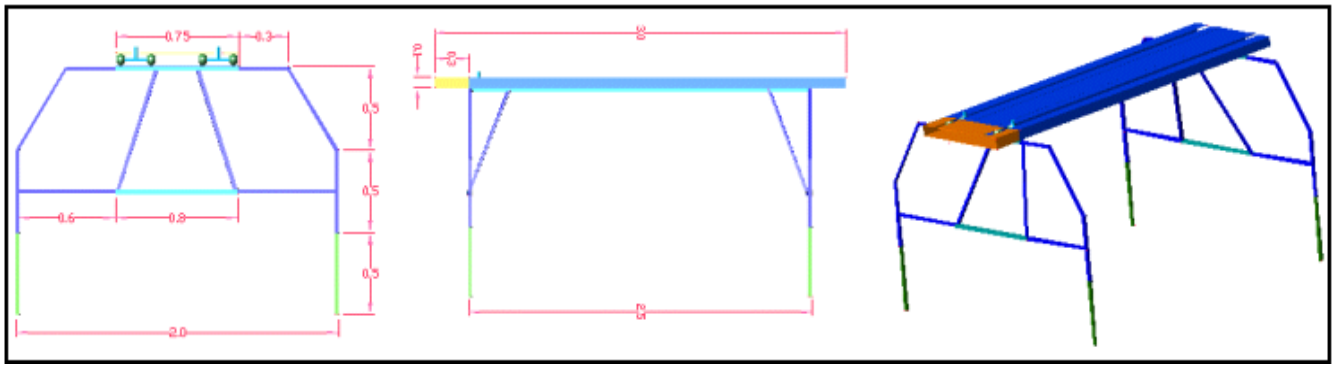

Figure 12. Detailed Drawing of Track System

4.5.4. *Track Subsystems*

Several logistic problems concerning the feasibility of the track system have been identified. These include transportation of the modular tracks, ability to assembly the system under harsh conditions, securing the system to the ground, and dust contamination of the wheel track wells.

Transportation of the module track system involves two aspects, transportation from earth and ease of transportation by crew. Since the weight and volume are critical attempts were made to produce a system that was volumetrically small and light in weight. To reduce the volume the system would take up during transport, the support legs of the track are collapsible, similar to the support legs found on folding tables.

In addition to transport to the planet, ease of transportation on the ground was considered. The track is designed for two persons to handle with ease. The width of the wheel track housing was limited to a width of 1 m for this purpose.

The set-up of the track system on Mars is designed to be completed by a two-person crew. Special consideration is given to the adverse terrain feature on Mars and the design of the track reflects this. The support legs of the track system are extendable in two axes to allow for modifications due to terrain. This will relieve the crew of moving large masses of soil or rocks to accommodate the track. The track supports are made of three different sized thin walled rectangular elements. The main support connects the track support to the wheel track. Outrigger supports are connected to the main supports and extend out and down from the main supports. The ground supports are adjustable legs perpendicular to the ground. Table 8 lists the track support names and their dimensions. The range of extension for the supports is 0.6 m parallel to the ground and 0.5 m perpendicular to the ground.

Table 8 Track Support Names and Dimensions

Support Name	Height x Width (cm)	Wall Thickness (cm)
Main	2.5 x 2.5	0.1
Outriggers	2.3 x 2.3	0.1
Ground	2.1 x 2.1	0.1

Track Ground Restraints

High winds are expected on the Martian surface. To restrain the track system from moving during high winds, ground restraints will be required. Adequate types of restraining mechanisms have not been investigated. However, a support structure, sufficiently driven deep into the Martian soil should secure the apparatus.

Modular Track Interface Feature

An interface has been designed to connect the modular track sections. The system consists of a male-female joining. The system works by fitting the end of one track into the supporting structure of another track. Each track contains a male and female connection.

Dust Contamination

Martian dust contamination will be a control problem for any sensitive apparatus operating on the surface. Dust control has been proposed to reduce the amount of dust that may enter the wells. The system consists of brushes that run the length of the opening of the carriage wheel structure. The brushes create a seal, restricting dust movement into the wells. As the wheel structure moves along the track, brushes will scrap dust way from the structure, further reducing contamination. One type of dust control will not be sufficient, however, and regular blowing of the track to displace dust may be required.

4.5.5. Design Limits

Carriage System

The carriage system has been designed to sustain a maximum landing load of four times the vehicle weight at a 60° glide path and a maximum deflection of 5cm.

Track System

The track system is designed to withstand a maximum 4G landing. The maximum deflection of the system is slightly less than the carriage system at 3 cm. The maximum deflection was decreased from the carriage system requirements to reduce cyclic vibration in the track while the carriage system is moving.

4.5.6. Factor of Safety for the Carriage and Track Systems

A large factor of safety was used to design the two systems. Normally, for an unmanned flight vehicle, a relatively low factor of safety between 1.0 and 1.2 is acceptable. However, due the extraordinary conditions that the system is to be used in and the distance from traditional repair facilities, a larger than normal factor of safety equal to 4 was used.

4.5.7. Material Selection for Carriage and Track Systems

The materials considered for the construction of the carriage and track systems consist of traditional aluminum alloy. The materials need to be light in weight, have good strength properties in bending, a minimum deflection under high loading, and desirable, a low cost. Aluminum alloy was found to closest meet these goals for both systems. Special consideration was made for the wheels of the carriage system. The wheels in the wheel carriage system could be made of polyurethane similar to the wheels found on commercial rollerblades™.

Material Properties

Table 9 is a list of the material properties for aluminum 6061-T6 used in this investigation.

Table 9 Material Properties for Carriage

Material	Density (Mg/m^3)	Young's Modulus (GPa)	Yield Strength (MPa)		
			Tension	Comp	Shear
6061-T6	2.71	68.9	255	255	131

4.5.8. Load Cases

Three load cases were examined to determine the configuration and cross-sectional element design of both the carriage and track systems. The load cases consisted of one 1G-load scenario and two 4G-load scenarios. The 1G load simulates the flight vehicle a rest. The 4G-load case examines a maximum landing scenario as described above. Two types of applied loads, a normal landing and a side-loading case were used. Normal landing loads are experienced when both wing supports are loaded at the same time. Side loading is experienced when one wing support is loaded before the other.

The weight component perpendicular (-y-axis) to the direction of travel was used. Loads parallel to the direction of travel (z-axis) were not considered. Any loads associated with the x-axis were not considered in this investigation.

The actual applied loads varied between the carriage analysis and the track analysis. For the carriage analysis, only the vehicle weight was used. For the track analysis, the vehicle weight and the weight of the carriage was used. For the 1G-load cases, the entire vehicle weight was used since the vehicle is at rest.

4.6. STRUCTURAL ANALYSIS OF THE WING

Accurate analysis of half of the MAEV wing body was done using MSC NASTRAN. A Finite Element Model (FEM) of half of the wing was constructed using rectangular bar-element for the ribs, membrane-element for the wing skin and plate-element for the circular spar. The wing section was then subjected to 2g loading to investigate its behavior under static and flight conditions. The materials used for the wing are Mylar Type A and Kevlar 149. Figure 13 shows the right half-span of FEM wing.

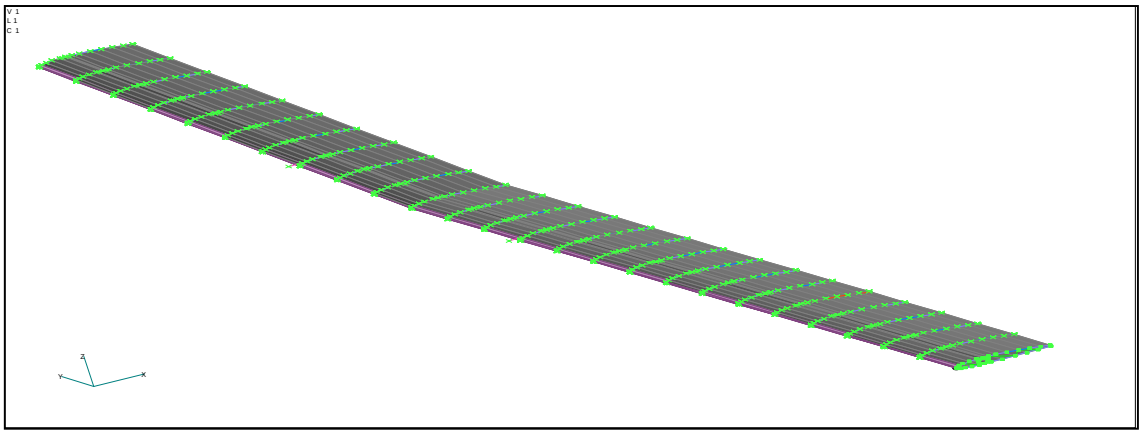

Figure 13. Right half span of FEM wing

4.6.1. Model

The wing has 6-degree dihedral on the 15th spar from the center as shown above. The main circular spar has diameter of 0.1 m from root to tip. It has two separate sections where the top and bottom wall thickness of 0.0012 m with 6 plies lay-up angle of [90/0/90]s2. Both sidewalls of the circular spar have a thickness of 0.004 m with 2 plies lay-up angle of [90/90]. The ribs are modeled as bar-elements, and have rectangular cross sections. They are placed 0.61 m apart of each other. The entire wing skin is made of a membrane-element and they carry only tensional load. Two types of material are used to construct of the wing. They are Mylar Type A and Kevlar 149. Two types of loading cases were considered and the behavior was analyzed using the Finite Element Method.

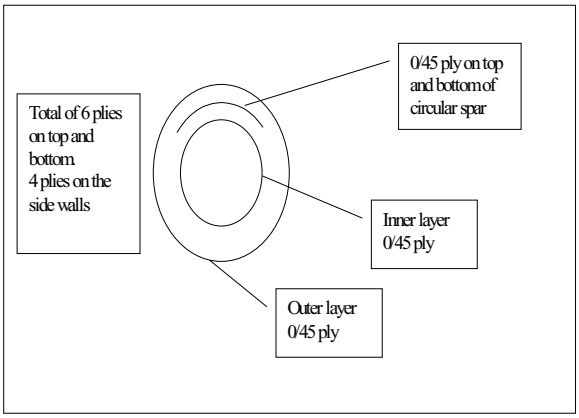

Figure 14. Main circular spar cross section

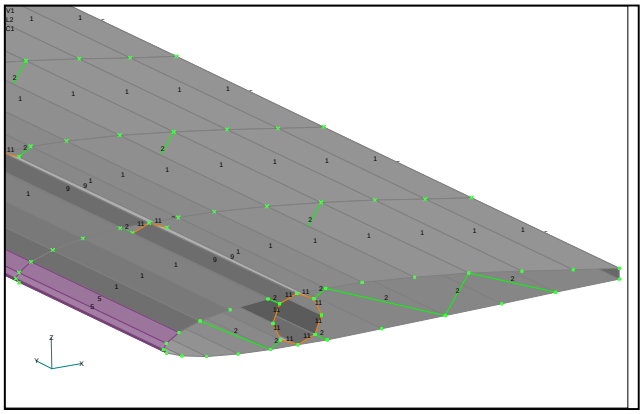

Figure 15. Cross-section of the wing

4.6.2. On Ground Case

For the On Ground Case, the aircraft is sitting still on ground and no aerodynamic force applies to it. The entire weight of the aircraft will be pointing downwards except for the landing gear and payload weight. The payload will be carried by the landing gear. The total downward force is 236 N. This causes reaction force of 236 N upward to fulfill the 'zero sum rule'. Figure 16 and 17 below show the wing loading and the deflection respectively, for half of the wing.

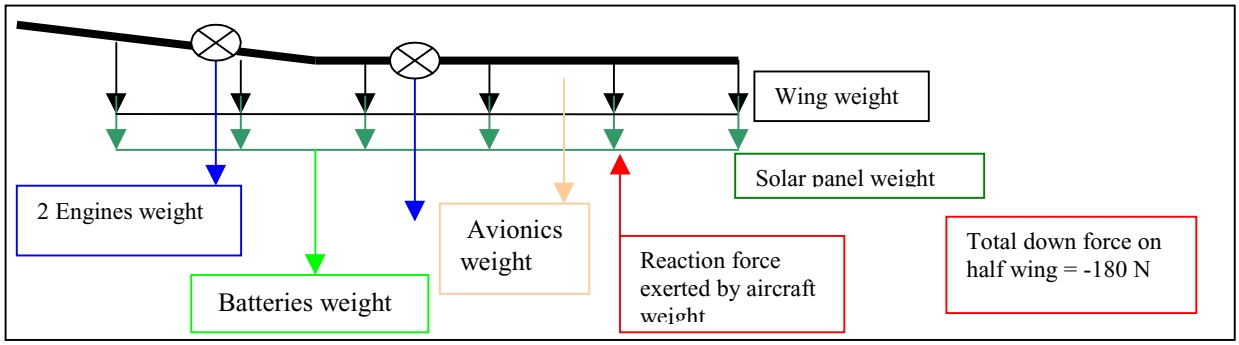

Figure 16. Load for On Ground Case (half wing shown)

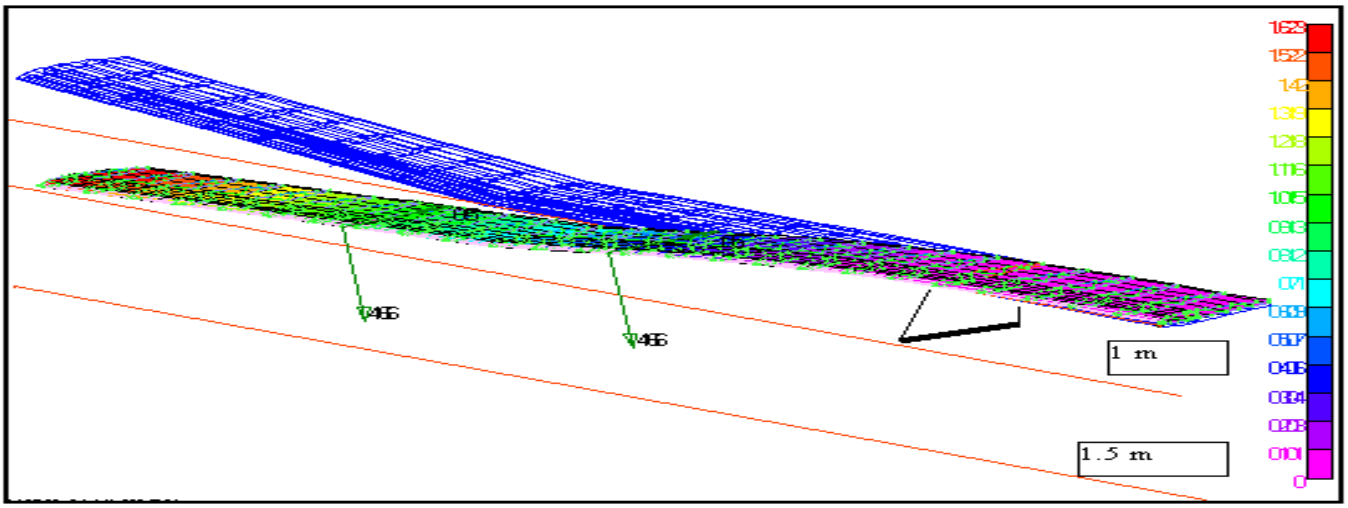

Figure 17. Deformation of wing On Ground Case

The wing deflection was calculated to be 0.68 meters downwards, which is small enough for the tip of the propeller blades to clear the ground by at least 1.0 meters. Stress analyses were done for the main circular spar, the ribs, the upper and lower skin and the leading edge using the same methods. The smallest margin of safety occurred on the bar-elements at 120%. The margins of safety for the other components were, however much higher.

4.6.3. In Flight Case

For the in flight case analysis, ideal and normal flying conditions were assumed. With the wing loading of 117 Newtons per half wing, the tip deflection was calculated to be 0.32 meters. Similar stress analyses were done for the in flight case and the smallest margin of safety occurred on the bar-elements at 200%. The other components resulted in much higher margins of safety.

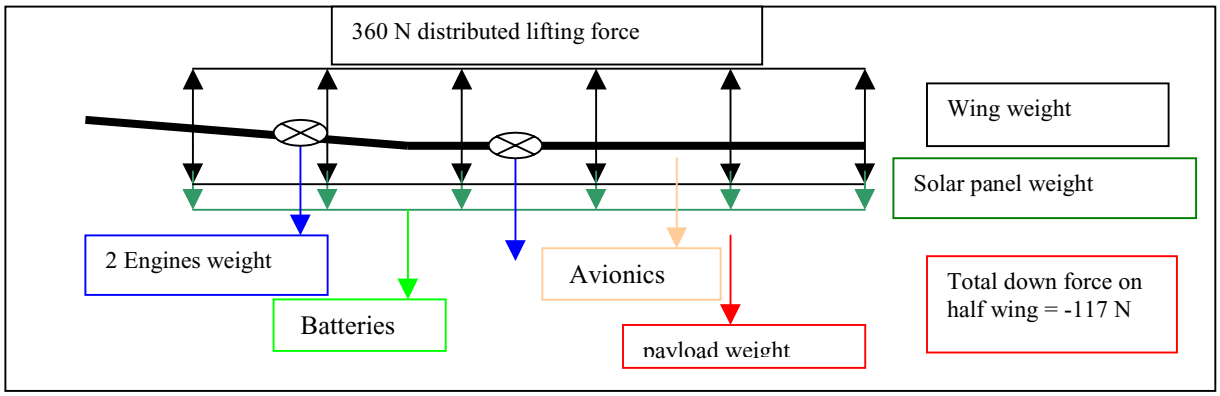

Figure 18. Loading for In Flight Case (half of wing shown)

4.7. Structural Analysis of Carriage and Track System

MSC NASTRAN software is utilized to analyze the structural models for the carriage system and the track system under the different load cases described above.

4.7.1. Analysis of Carriage System

The carriage models are constructed using solid, thin walled circular beam elements. Eight constraints are applied to simulate the carriage wheels. Loads are applied to the peripheral of the wing supports at 24 nodal point per wing support.

4.7.2. Four G NASTRAN Analysis of Carriage Support

Side Loading

The 4G-side loading yielded the largest elements stresses and deflections. This load scenario was used to determine the geometry of the structure and the element thickness'. The vector weight component of the vehicle was divided into 24 nodes and applied to the right wing support. The nodal loads are 43.3 Newton's each.

The individual elements of the carriage system are separated into five different material properties; each associated with a subsystem. In NASTRAN, a material property identifies an element material and cross-sectional

geometry. For the truss subsystem, two material properties were used to increase the options for individual element sizing. The wheel support subsystem contains one material property and the wing support subsystem contains two material properties. Table 10 lists the material properties, the subsystem they are associated to, and the element geometry.

Table 10. Material Property Definition

Property Name	Subsystem	Geometry	Radius(cm)	Thickness(cm)
Truss	Truss	Thin-walled circle	1.0	0.2
TrussA	Truss	Thin-walled circle	0.5	0.2
Wheel	Wheel	Thin-walled circle	1.5	0.1
Wing Support	Wing Support	Thin-walled circle	2.0	0.2
Stringer	Wing Support	Solid circle	0.1	N/A

The analysis of the carriage system with the defined material properties yields an acceptable deflection of 5.0 cm. The maximum combined element stress is 144 MPa. The combined stress is defined as a combination of the bending stress and the axial stress. The largest stresses were experienced in the elements of the wheel subsystem. Bending stress largely influences the maximum combined stress. The wheel support elements are nearest the constraints and furthest from the applied loads, experiencing the largest reaction moments.

The maximum allowable deflection was the limiting factor in the design consideration of the carriage system. In meeting the maximum deflection criteria, the allowable yield stress for aluminum 6061-T6 were easily satisfied. The largest stress in an element was 144 MPa, just over half the allowable yield stress for the material. With the structural geometry given, the total mass of the structure was calculated to be 26.45 kg.

Normal Landing

A 4G normal landing load case was analyzed to confirm that deflections and element stress did not exceed design limits. The maximum deflection for this scenario is 2.13cm and the maximum combined stress is 78.05 MPa. All elements meet the allowable yield strength for aluminum 6061-T6.

4.7.3. One G NASTRAN Analysis of Carriage Support

A 1G NASTRAN analysis of the carriage system to simulate the vehicle at rest on the carriage system was conducted. This investigation identified the deflection and stress of the carriage system due the weight of the vehicle only. The carriage system deflection is 0.75 cm and the maximum combined stress is 27.1 MPa. All elements meet the allowable yield stress for the material.

4.7.4. Results of carriage Analysis

Table 11 is a reference table listing the results of the structural analysis for the carriage system. The three load case scenarios are listed with the maximum deflection and element stresses. All design limits are satisfied for the load cases investigated.

Table 11. Results of Carriage System Analysis

Load Case	Deflection (cm)	Maximum Combined Stresses (MPa)
4G-Side Loading	5.1	144
4G-Normal Landing	2.1	78.5
1G-Normal Landing	0.75	27.1

4.8. ANALYSIS OF TRACK SYSTEM

The same load cases for the carriage system were used to investigate the track system. These load cases consisted of a 4G landing case and a 1G wing weight only case. For the 4G-load case, side loading and normal landing scenarios were investigated. NASTRAN was used to examine the structure for maximum combined stress in the supports and principal (Von Mises) and shear stresses in the plate elements of the track.

4.8.1. 4 G Hard Landing

Side-loading

Similar to the carriage system analysis, the 4G side-loading scenario yielded the highest element stresses and largest deflection. This load scenario was used to satisfy the design requirements. The NASTRAN analysis of the track system contains two different types of element properties. The track supports, as described above, are thinned-walled rectangular beam elements. The main track is modeled as thin plates. The analysis of the track system identified the maximum required thickness for both the beam elements and the plate elements.

Similar to the carriage system, the maximum allowable deflection was the limiting factor in the design of the track system. The largest element stresses were experienced in the track supports. The maximum combined stress is 113.1 MPa.

The maximum Von Mises stress is 96.1 MPa. The maximum shear stress is 34.6 MPa for the main track. All elements in the analysis meet maximum allowable stresses for the material.

The total deflection for the track system for a 4G side loading case is 2.8 cm. The total mass for the apparatus is 15.56 kg.

Normal Landing

A 1G normal landing analysis was conducted to simulate the weight of the vehicle and the carriage on the track at rest. The maximum deflection is 1.3 cm. The maximum combined stress for the support subsystem is 61.0 MPa. The maximum Von Mises and shear stresses are 39.1 and 14.1 MPa, respectively. All elements meet maximum allowable material strengths for aluminum 6061-T6.

4.8.2. 1G Normal Landing

A 1G, vehicle and carriage mass only analysis was performed to identify the maximum deflection of the system while at rest. The maximum deflection of the apparatus while at rest is 0.47 cm. All structural elements maintained a substantial factor of safety for allowable stress values.

4.9. Results of Track system Analysis

The result of the track analysis is presented in Table 12. The maximum deflections and stresses of each load case scenario are presented. The design limits are satisfied for all load cases.

Table 12. Results Track System Analysis

Load Case	Deflection (cm)	Maximum Element Stresses (MPa)		
		Von Mises	Shear	Combined
4G-Side Loading	2.8	96.1	34.6	113.1
4G-Normal Landing	1.3	39.1	14.1	61.0
1G-Normal Landing	0.47	14.2	5.1	22.2

4.10. Take Off Analysis

To enable the MAEV to takeoff safely in a short track distance, the carriage system can be designed to accommodate two progressive rockets for additional thrust. Selecting a form of solid rocket booster that can provide progressive thrust, the takeoff process can be initiated with a small thrust vector to avoid structural damages to the aircraft and the Carriage. A quick analysis was done using rocket boosters composed of Polysulfide Aluminum and Ammonium Perchlorate (PS/AL/AP) grains weighing 22 Newtons each. Initially, each rocket booster can generate about 296.42 N of thrust, which increases progressively over time. As required from performance, the aircraft needs the lift-off velocity at 36.3 m/s to be airborne. At the time of 19.05 second, the maximum thrust is 1779.0 N, which gives the aircraft a velocity of 37.36 m/s. This velocity is slightly greater than required velocity, which intends to ensure the aircraft to generate enough lift. The resulting take-off distance is approximately 30 meters. To simplify the calculations, the drag and friction on the track are ignored and the total combined weight of the MAEV and the Carriage is 400 N. The linear dimension of each booster will be at least 0.5 meters. The inner and outer cross sectional diameter for the grain will need to be approximately 0.015 and 0.09 meters respectively to accommodate enough grain volume for a successful takeoff.

These boosters can be attached to the Carriage system instead of the aircraft, which eliminates excess weight of the boosters after they are used up, and will also avoid possibilities of exhaust blast damage to the wing. The thrust output of the rockets can be varied to satisfy any type of take off requirements.

4.11. Landing Simulation

From the principle of work and energy, the average horizontal acceleration of the MAEV is $3.96 m/s^2$ during touchdown. The MAEV, which moves along with the carriage on the landing track applies a load factor of 1.11g.

The horizontal g-forces after impact is 2.13g, which slowly decreases with the spring force. The kinetic friction of the track also provides resistance. The combined effect of the spring and the spool mechanism halt the MAEV in just 60-meter. This is assuming that the landing speed of the MAEV is 10% of the stall velocity (30m/s) or 33m/s ($1.10V_{stall}$). Figure 19 (a to d) shows the sequence of the MAEV landing on the carriage and track system.

Figure 19(a) shows the setup before the aircraft comes into contact with the carriage. The fundamental mechanisms include a spring, spools and an inelastic wire. It also shows the carriage rushing to make contact with the

wire, assuming a landing approach from the right. Side view of the spools shown in the right, indicates the wire in tension both at top (colored in orange) and bottom (colored in blue) of the spool. The spring is shown in static equilibrium.

Figure 19(b) shows the moment after the carriage comes in contact with the wire. The wire is designed to feed out turning both the top and bottom spools. The wire, which is connected to the spring, causes it to compress. Recall that the spring is designed to provide resistance force during the MAEV landing process.

Figure 19(c) shows the stage when the MAEV is brought to a complete stop. The wire is fed by the top spool is relaxed. The bottom spool, however, remains locked, storing the kinetic energy as potential energy in the spring.

Figure 19(d) shows the release of the stored potential energy from the spring as the top and bottom spool wind in. The force of the spring is also designed to assist in "pushing" the carriage back towards the takeoff position, which is at the right end of the track diagram shown below. The purpose of this design is to allow the aircraft to take off and land in the same direction.

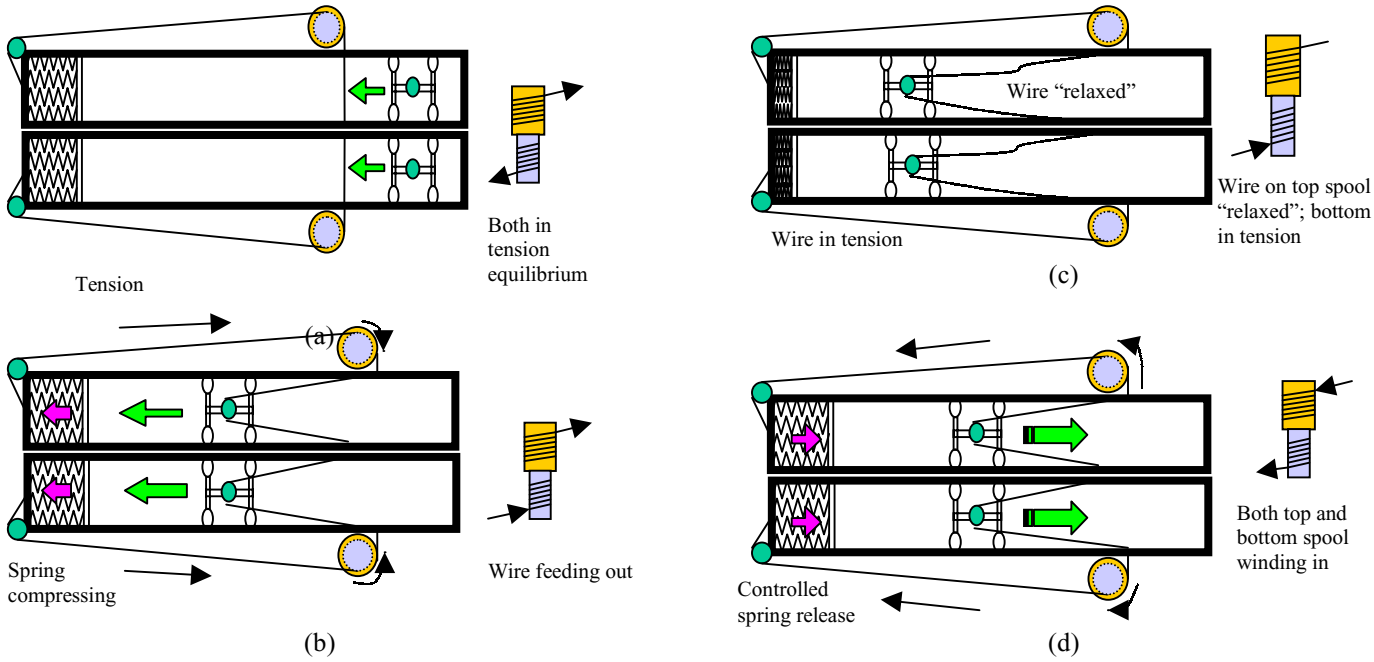

Figure 19. Process of landing using spring and spools mechanism with wire

4.12. MARS EXPLORATION PARACHUTE

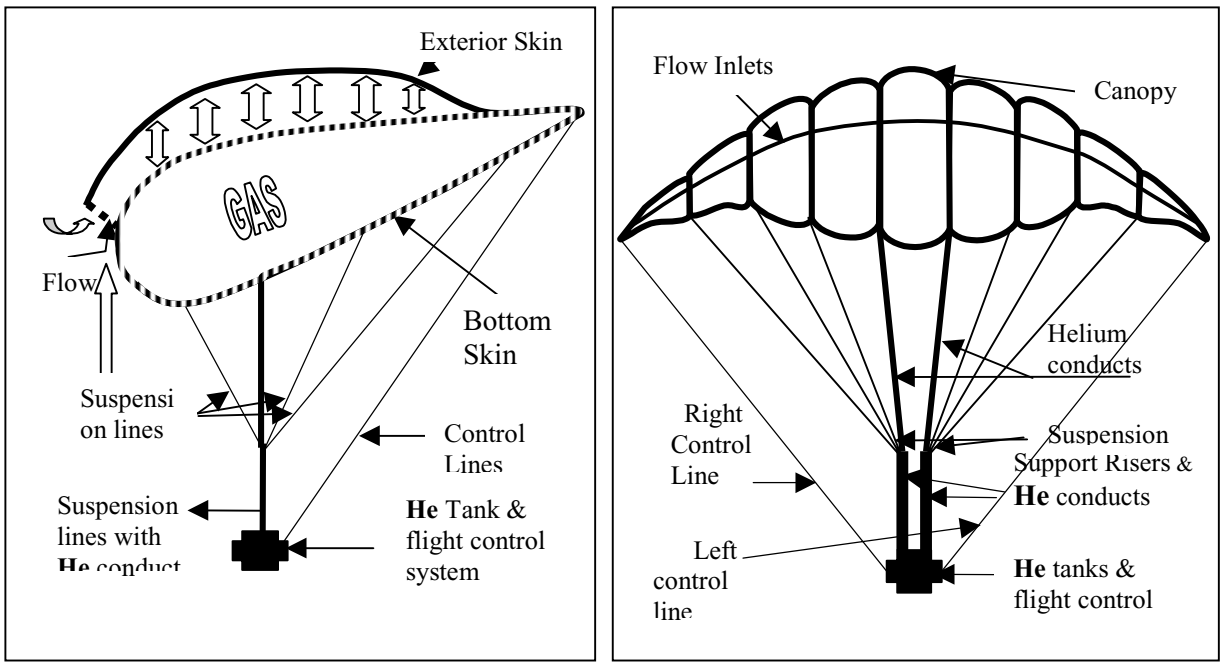

Figure 20. View of the parachute payload

The *Mars Exploration Parachute* is the combination of an aerostatic balloon (filled with a lifting gas, such as helium or hydrogen) in combination with a ram-air or gliding parachute. As a balloon, it is able to ascend and descend at specific rates depending on the controllable amount of gas flowing in and out of the envelope. As a gliding parachute, it meets all the design criteria to be classified as a wing of variable shape with specific aerodynamic characteristics.

The canopy is made of three skins, an upper skin and a double lower skin. The upper skin preserves pressurization inside when it is descending by means of several flow inlets located at the nose of the parachute. The inner skin preserves the wing-like shape of the parachute when gas is pumped in. A set of lines cascade from the top to a small payload located at the bottom, consisting of a guidance and automatic control, a small digital camera, and all necessary electrical and telecommunications devices. Figure 20 of the parachute show the front and profile views of the structure.

The *Mars Exploration Parachute* is intended to function in two different ways:

a) To be released from high altitude and glide to the surface. The more important issues involved this case are the opening peak force of the parachute when it deploys, the rate of descent, and the landing velocity conditioned by the buoyant force of Helium.

b) To be released from a lower altitude and land it by means of airbags and retrorockets. In this case, the parachute deploys automatically on the ground and Helium provides the necessary lifting force. Once the system has acquired the desired altitude, the Helium supply is stopped and the parachute starts its descent, releasing gas and obeying the basic aerodynamic laws.

In any case, when a specific spot is sighted via digital camera, the canopy is directed towards that location with an automatic system that drives the control lines, which deflect part of the canopy just as a regular flap of a rigid wing. Since the motion of the system is expected to be slow, only static stability is of concern, achieved through the length of the control lines supporting the payload.

Since the atmosphere is so frigid and thin, a large quantity of Helium is necessary to lift the payload, and therefore extraordinary wing dimensions are expected. A brief study was performed based on several calculations. Table 13 below lists the major specifications of the parachute payload.

Table 13. Parachute design specifications

NACA-4415	
C_L max	1.1
C_L with flaps	2.5
$C_{d,o}$	0.015
Reynolds number	$5x10^5$
Mach number	04-0.6
Weight of system	15 N
Wing span, b	28
Wing chord, c	11
Wing average height	1.5
Wing volume	460 m^3
Wing area	308 m^2
Wing aspect ratio	2.54
Wing loading	0.048
Flight path angle	15 °
Lift to Drag ratio, L/D	~4

5. Conclusions

The optimal configuration for the MAEV was determined. The flying wing configuration is a span of 30.5 meters and a chord length of 1.2 meters. Four propellers driven by electric motors power the aircraft. A solar array on the upper surface of the wing and six rechargeable batteries supply power for the motors and all systems. The MAEV will be able to accomplish its mission objectives over a nine-hour flight time and maximum range of 1000 km. The optimum cruise velocity of the aircraft is 66m/s at a maximum altitude of 500 m.

The modular track and carriage system will assist the MAEV with take-off and landing. The overall length of the track is 60m. Two solid rocket boosters mounted to the carriage and the resistance pulley mechanism will assist the aircraft in the take-off and landing process respectively. The track and carriage systems have been designed to be ergonomically suitable for a two-man crew.

6. Recommendations

For future academic research on the report presented, several recommendations have been proposed. A process of modularizing the entire aircraft, carriage and track system needs to be developed for transportation to and on the Martian planet. To further improve the performance of the MAEV, several areas can be researched.

These include:

- Design a better, more suitable propeller with lower Reynolds numbers
- Conduct a thorough stress analysis during takeoff and landing condition
- Use of alternative materials to construct the Track & Carriage and some components of the aircraft.
- Develop avionics and control systems appropriate for a wing body design
- Research on higher efficiency solar arrays and batteries
- Additional loads applied to the Track and Carriage system need to be considered
- Find alternative methods to assist in the takeoff and landing process of the MAEV
- Do a cost analysis and a feasibility study to recommend further development on this design

By following these recommendations, the overall functionality and the possible reality of the Martian Airborne Exploration Vehicle and the Carriage & Track system can be greatly improved.

7. Outreach

In April of this year, the Wichita State University College of Engineering held its annual Open House. The MAEV group participated in this event. The daylong event allowed varies engineering disciplines to present their semesters work. The event is attended heavily by both the industry and local elementary schools. Presenting to local industry engineers allowed the MAEV group to refine their technical presentation. Presenting to the school groups allowed the MAEV group to garnish the interest of the next generation.

Future plans for the MAEV project consist of presenting the model and a brief description of our work to Wichita's newest science learning center, Exploration Place. Exploration Place is an interactive learning environment for children of all ages. It is our hope that the MAEV project will be awarded a place on permanent display, so that children and grown-ups alike can come to understand the possibilities in the new frontier.

8. Bibliography

Allen, David H. and Walter E. Haisler, "Introduction to Aerospace Analysis", John Wiley and Sons, 1985

Hibbeler, R.C, "Statics and Mechanics of Materials", Simon & Schuster, 1993.

Lacy, Thomas E. Jr., "Aerospace Engineering Flight Structures Class", Wichita State University, 1998-99, Wichita KS

Boresi, Schmidt, and Sidebottom, "Advanced Mechanics of Materials", 5th Edition, John Wiley and Sons, 1932.

Bruhn, E.F., "Analysis and Design of Flight Vehicle Structure," Jacobs Publishing, Inc., 1973.

Dommasch, Daniel O., Sherby, Sydney S. and Connolly, F. Thomas, "Airplane Aerodynamics", 4th edition, Pitman Publishing Corporation, NY, 1967.

Durand, W. F, "Aerodynamic Theory", vol. I, Durand Reprinting Committee, Galcit, 1943.

Michael A. Dornhem, "Aviation Week & Space Technology, AeroVironment Pushes Limits of Solar Flight", May 1998.

Fishbane, Gasiorowicz, "Physics for Scientists and Engineers", 2nd ed. New Jersey: Prentice Hall, 1996.

R. C. Hibbeler, "Engineering Mechanics, Dynamics", 7th ed. New Jersey: Prentice Hall, 1995.

John D. Anderson, "Introduction to Flight", 3rd ed. New York: McGraw Hill, 1989.

Fishbane, P. M., "Physics for Scientists and Engineers", Prentice Hall, 2nd ed, 1996, pp. 12-614.

Chenming Hue and R.M.White, Solar Cells From Basic To Advanced Systems, McGraw-Hill, New York, 1983.

H.S.Rauschenbach, Solar Cell Array Design Handbook, Van Nostrand Reinhold, New York,1980.

K.Zweibel, Basic Photovoltaic Principles and Methods, Van Nostrand Reinhold, New York,1984.

Martin A.Green, Solar Cells;Operating Principles, Technology and System Application, Prentice Hall, New Jersey,1982.

Robert G.Seippel, Photovoltaics, Reston, Prentice Hall, Virginia, 1983.

Anthony J.Colozza, "Preliminary Design of a long-Endurance Mars Aircraft," NASA CR 185243, http://powerweb.lerc.nasa.gov/psi/DOC/mppaper.html

Anonymous, "Flexible Thin Film Solar Cells," NASA SBIR./STTR

http://sbir.gsfc.nasa.gov/SBIR/successes/ss/3-027text.html

Dale Burger, "Mars Microrover Power Subsystem," Mars Pathfinder Microrover http://192.88.114.52/Mars/roverpwr/power.html

Anonymous, "Pathfinder Leading the Way In Solar Flight," Pathfinder Fact Sheet http://www.dfrc.nasa.gov/PAO/PAIS/HTML/FS-034-DFRC.html

Geoffrey A.Landis, "Solar Cell Selection For Mars," Solar Cell Selection for Mars http://powerweb.lerc.nasa.gov/pvsee/publications/wcpec2/cells4mars.html

Anonymous, "Solar Cell Efficiency Records," Photovoltaics Special Research Center http://www.pv.unsw.edu.au/eff/eff_tab1.html

Kirk Flittie and Bob Curtin, "Pathfinder Solar-Powered Aircraft Flight Performance," AIAA-98-4446

Anonymous, "New World-Record Efficiency in Thin-Film Solar Cell," National Center for Photovoltaics" Anonymous, "Function and Performance of Lithium/Thionyl Chloride Cells," Function and Performance of Lithium/Thionyl Chloride Cells http://www.batteryeng.com/func_perf.htm

Anonymous, "Lithium/Thionyl Chloride Batteries," Application Overview- Lithium/ Thionyl Chloride Batteries http://sonnenschein-lithium.de/Applicat/applltc/overview/Overview.htm

Anonymous, "Rechargeable Solid State Battery," SBIR/STTR http://sbir.gsfc.nasa.gov/SBIR/successes/ss/105text.html

Brown, C.D., Spacecraft Propulsion, AIAA, 1996, pp. 9-212.

Hill, P. and Peterson, C., Mechanics and Thermodynamics of Propulsion, 2nd ed., Addison-Wesley, 1992, pp.469-612.

Sutton, G. P., Rocket Propulsion Elements, John Wiley & Son, 3rd ed., 1963, pp. 310 – 386

McGettrick, Mike, "AE660N Finite Element Modeling Class", Wichita State University, Jan - May 2000

Smith, Bert, "AE653 Introduction to Composite", Wichita State University, Sept.- Dec. 1999.